

A SPECTROMETER FOR DOUBLE-DIFFERENTIAL NEUTRON-EMISSION CROSS SECTION MEASUREMENTS IN THE ENERGY RANGE 1.6 TO 16 MeV

Erik DEKEMPENEER and Horst LISKIEN

Commission of the European Communities, Joint Research Centre, Geel Establishment, Central Bureau for Nuclear Measurements, B2440, Geel, Belgium

Louis MEWISSEN and Freddy POORTMANS

S.C.K./C.E.N., B2400, Mol, Belgium

Received 13 October 1986 and in revised form 18 December 1986

A neutron spectrometer for the measurement of double-differential neutron-emission cross sections has been set up.

An electron linac (GELINA) is used as a pulsed white neutron source. The energy of the incident neutrons is determined by the time-of-flight method. The secondary neutron spectra are determined by unfolding the pulse-height distributions observed in eight NE213-scintillators surrounding the sample.

The measured spectra are normalised to the shape of the incident neutron flux measured with a ^{235}U -fission chamber, and afterwards converted to absolute cross sections using as standard the carbon differential elastic scattering cross section below 2 MeV.

1. Introduction

Experimental data on double-differential neutron-emission cross sections are requested for the conceptual design studies of a blanket of a DT-fusion reactor [1–4] and are important for a better understanding of the reaction mechanism, in particular for the pre-equilibrium neutron-emission process.

Up to now most of the data measurements were performed with pulsed monoenergetic neutron sources so that the secondary neutron energy can be determined by time-of-flight. To cover the incident neutron energy range from 1 to 16 MeV required for fusion technology applications, this is a very time consuming method and for that reason the existing data base is rather poor. The experimental method described here uses a pulsed white neutron source and therefore is much more efficient in obtaining data. White source experiments have already been performed on a few elements at Oak Ridge [5] but the sample-detector geometry was such that measurements for only one angle at a time were possible. With our experimental setup it is possible to obtain data for 8 angles simultaneously.

2. Experimental method

2.1. General description

The spectrometer is installed at the pulsed white neutron source of the linear electron accelerator at the

C.B.N.M. The machine is operated at a repetition rate of 800 Hz with an average total beam power of 8 kW and an electron burst width of less than 1 ns [6]. Neutrons are produced via (γ, n) and (γ, F) reactions in a mercury cooled rotary uranium target [7]. A target consisting of a U-Be mixture which will produce a harder neutron spectrum, is under construction. The neutron beam is collimated to a diameter of 5 cm by two pairs of Pb (10 cm thick) and Cu (20 cm thick) collimators installed at 30 and 54 m from the neutron source. These are surrounded by a large mass of sand to absorb the scattered neutrons. A depleted uranium filter, placed at the 30 m station, attenuates the flash of gamma rays arising from the electron bombardment of the U-target. Its thickness depends on the Z-value and the total weight of the scattering sample and is typically about one cm. Moreover, we have shielded our flight-path against the water moderator in the target bunker which produces most of the low-energy neutrons, so that no overlap filter is needed.

The scattering sample, cylindrical in shape ($\varnothing = 7$ cm) with axis parallel to the incident neutron beam, is positioned at 60 m from the neutron source. It is mounted in an aluminium vacuum tube to reduce air-scattering of the incoming neutrons and to prevent possible oxidation of the sample (fig. 1). The secondary neutrons are detected with eight proton-recoil liquid NE213-scintillators (BA1-type cell, $\varnothing = 5$ cm, $h = 5$ cm), directly coupled to RCA8850 photomultipliers without magnetic shield. Special care was taken to

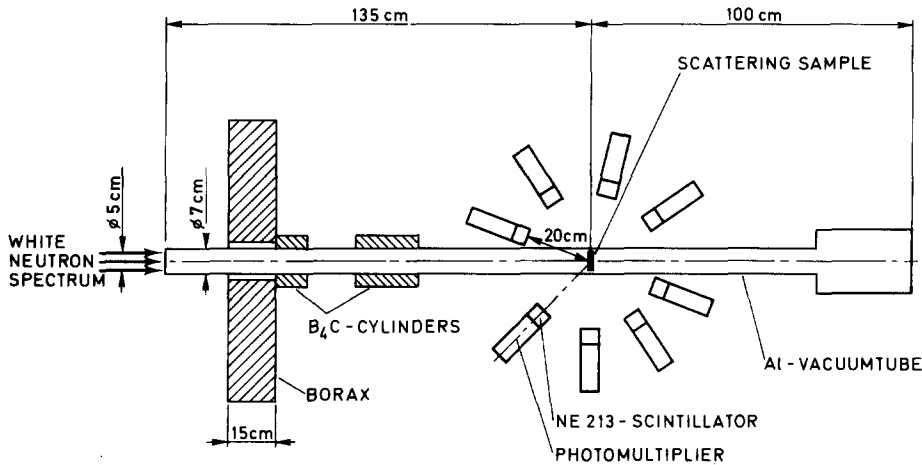


Fig. 1. Diagram of the neutron spectrometer at the 60 m station.

minimize the amount of aluminium used in the detector canning which is small compared to the amount used in the commercial BA1-type cell itself. The detectors surround the sample at a distance of 20 cm at emission angles ranging from 20° to 160° . At larger distances, smaller forward and larger backward angles can be reached. Pulse shape discrimination, based on the charge comparison method, is applied to separate neutron from gamma events.

The incident neutron energy is determined by the time-of-flight method, in which the stop signal is derived from the detection of a secondary particle or gamma ray. This method provides an accurate measure of the real flight-time since the distance covered by the secondary particles (20 cm) is negligible compared to the flight-path length of the incident neutrons (60 m) (about 1100 ns are required for a 16 MeV neutron to traverse 60 m, whereas a 1 MeV scattered neutron needs only 14 ns to travel from sample to detector). The secondary neutron energy is determined by unfolding the pulse-height distributions as observed in the scintillators. The response matrix which is used to unfold the spectra is discussed in section 3.

The major source of background is due to scattering of the incoming neutron beam by the thin windows (0.3 mm thick) of the aluminium vacuum tube in which the sample is mounted and by the collimators. This contribution is kept low by using a long tube (235 cm) so that the window-detector distance is much larger than the sample-detector distance, and by the installation of a 15 cm thick borax shield and two B_4C cylinders (cf. fig. 1). Background coming directly from the neutron source is negligible due to the large distance between source and detectors. This is an important advantage of our method over the experimental conditions when using monoenergetic neutron beams produced with a Van de Graaff accelerator where the source-detector distance is of the

same order as the sample-detector distance (typically a few meters). This sample-independent background is accurately measured with a dummy vacuum tube (section 5) and is so low that we can use very thin samples (transmission > 0.9). Moreover, this background yields a pulse-height spectrum which extends above the pulse-heights coming from the neutron-emission of the sample. So the normalisation of the background to the foreground can be performed on this upper part of the pulse-height spectrum as well as with respect to the number of incident neutrons. The sample-dependent background can not be measured but the experimental results demonstrate that it amounts to only a few percent of the total secondary neutron yield (section 5).

At 60 m from the neutron source the difference in flight-time between the gamma-flash (gamma rays coming directly from the target) and a 16 MeV neutron is only about 900 ns. Therefore, to avoid distortion of the amplitude signals by a gamma-flash pulse we can only accept one event per burst. Typically, about 30% of the linac bursts is lost due to this precaution.

During the scattering experiment the shape of the incident neutron flux is measured with a multiplate ^{235}U -fission chamber which is mounted in the neutron beam at 100 m from the neutron source. This chamber contains 2.5 g of ^{235}U (average layer thickness is 1.18 mg/cm²) and operates with continuous methane flow at atmospheric pressure [8]. With such thick layers we obtain a sufficient count-rate (0.05 events per burst) but special care must be taken to discriminate against the pileup pulses due to the α -decay of uranium.

2.2. Electronics and data acquisition system

For reasons explained in the previous section, we accept only one event per burst. Each time an event is detected, four signals are transferred to a HP 1000F

MeV. The bin width of the incident energy groups ranges from 0.2 MeV at 2 MeV to 1 MeV at 16 MeV. This three-dimensional array occupies $8 \times 32 \times 2048$ words in the central memory.

During the experiment the contents of several counters recording the number of linac bursts, the number of counts in a BF_3 monitor located in the target bunker, the number of events stored in the three-dimensional data histogram, the number of gamma rays detected, the number of coincidences or gamma-flashes that occurred, are listed every 30 min. These listings enable us to follow up the experiment on-line and are useful for the off-line data reduction.

3. Detector calibration

3.1. General

Since the secondary neutron energy is determined by unfolding the pulse-height distributions, it is important to know accurately the response functions of our scintillators. The accuracy of calculated response functions using the Monte Carlo method strongly depends on the uncertainties in the nuclear data base used and on the accuracy with which the light output function of the charged particles is known. Therefore we have performed an experimental calibration of a NE213-scintillator. The experimental details and the results from a comparison with calculations using the codes NRESP4 and NEFF4 [9] are discussed in the following sections.

3.2. Relative response functions

We have measured pulse-height distributions as a function of energy by placing a detector in the direct neutron beam of GELINA (at the 400 m station) with its axis parallel to it. The collimators, which reduced the beam diameter to 7 cm at 400 m, were located at 100 and 200 m from the neutron source so that background due to neutron scattering in the collimators was negligible. The room background was already thoroughly investigated in connection with transmission experiments performed at this 400 m station. Even without rejecting the gammas this contribution is only in the order of 0.1% at 1 MeV and 1% at 16 MeV [10]. A 6 cm depleted uranium filter was used to attenuate the neutron beam sufficiently in order to avoid pileup of pulses. A similar data acquisition system as described in section 2.2. was used. In this case the TD was adapted to accept more than one event per burst. The time-of-flight spectrum was compressed on-line in 254 groups. The corresponding energy groups were regularly spread between 0.3 and 16.2 MeV with bin widths ranging from 0.02 to 0.15 MeV. Their pulse-height distributions were stored in the central memory of the computer in 2K spectra

each. Below 700 keV proton energy a perfect discrimination between neutrons and gamma rays was no longer possible. The neutron-gamma ray separation line was set in such a way that 5% of the photo-electric peak of the 60 keV γ -line of an ^{241}Am source was counted as neutrons.

Such an extensive set of response functions enabled an accurate determination of the proton light output function $L_p(E)$ for our scintillator. The "light unit" of pulse-height was defined such that the half-height of the Compton recoil edge for the 1.1155 MeV gamma rays from ^{65}Zn occurs at 0.920 light units. This corresponds with an electron light output $L_e(E) = a(E - E_0)$, where $E_0 = 0.005$ MeV and $a = 1$ MeV $^{-1}$, if one assumes that the true Compton edge lies 2% below the half-height of the Compton recoil edge [11]. First, L_p -values were estimated from the position of the half-height of the upper edges of the measured spectra. Afterwards, a smooth fit through these points was used to construct a table of light output values which we could introduce in the Monte Carlo calculations. This table then was adjusted in order to optimize the agreement between the measured and calculated spectra. Above 700 keV, the criterion was that the position of the upper edges of the spectra should coincide within 1%. Below this threshold the measured spectra are distorted due to an imperfect pulse shape discrimination, which makes it difficult to define accurately the upper edge. The light output for these lower energies was adjusted indirectly by comparing measured and calculated spectra for higher energies. Indeed, these spectra are sensitive to the low energy light output values through the multiple scattering effect in the scintillator. In the calculations, the light output functions for the other charged particles (d, α , Be, B, C) were taken from ref. [9] (1). The coefficients in the relations for the α -particle were adapted so that the structure induced by the $^{12}\text{C}(n, \alpha)^9\text{Be}$ interaction in the 9 MeV response function occurred at the correct position. At this energy the $^{12}\text{C}(n, \alpha)^9\text{Be}$ cross section is well known [12].

$$\begin{aligned} L_d(E) &= 2L_p(E/2) \\ L_\alpha(E) &= 0.02017E^{1.871} & E < 6.76 \text{ MeV} \\ L_\alpha(E) &= -0.6278 + 0.1994E & E \geq 6.76 \text{ MeV} \\ L_{\text{Be}}(E) &= 0.013E \\ L_{\text{B}}(E) &= L_{\text{C}}(E) = 0.0097E \end{aligned} \quad (1)$$

The pulse-height resolution $\Delta L(\text{fwhm})$ used in the calculations was described by a pulse-height dependent resolution-function [13].

$$\Delta L = (\mu^2 L^2 + \beta^2 L + \gamma^2)^{1/2}. \quad (2)$$

This relation describes the detector resolution due to various effects:

Table 1

Proton light output function, $L_p(E)$, for a NE213-scintillator. The function is described by a set of six polynomials of third order. In the table we have listed the coefficients A_0, \dots, A_3 for the six proton energy intervals. Special care was taken to obtain a good continuity for $L_p(E)$ and its derivative.

| E_p (MeV) | 0.0–0.4 | 0.4–1.1 | 1.1–3.0 | 3.0–6.4 | 6.4–8.9 | 8.9–16.0 |
|----------------|---------|----------|----------|----------|----------|----------|
| A_0 | 0.0 | 0.00829 | -0.02060 | -0.07129 | 3.85138 | -0.76801 |
| A_1 | 0.06798 | 0.01275 | 0.09088 | 0.18958 | -1.36975 | 0.57306 |
| A_2 | 0.06034 | 0.18149 | 0.11066 | 0.06138 | 0.26122 | 0.0 |
| A_3 | 0.05527 | -0.03206 | -0.01055 | -0.00326 | -0.01138 | 0.0 |

- (a) the locus-dependent light transmission from the scintillator to the photocathode (first term),
 (b) the statistical effects of the light production, attenuation, photon to electron conversion and electron amplification (second term),
 (c) all noise contributions (third term).

The upper edges of the experimental response functions were best reproduced using the values $\mu = 0.045$, $\beta = 0.075$ and $Y = 0.002$. In table 1 we present a polynomial

fit to the adjusted proton light output values. This fitting has introduced an additional uncertainty of only 0.1%.

Fig. 3 shows a comparison between measured and calculated spectra. In the region where the pulse shape discrimination is excellent ($E_p > 700$ keV) the calculations reproduce very well the proton-recoil plateau but fail to explain the structure induced by α -producing reactions with carbon in the scintillator. The latter is

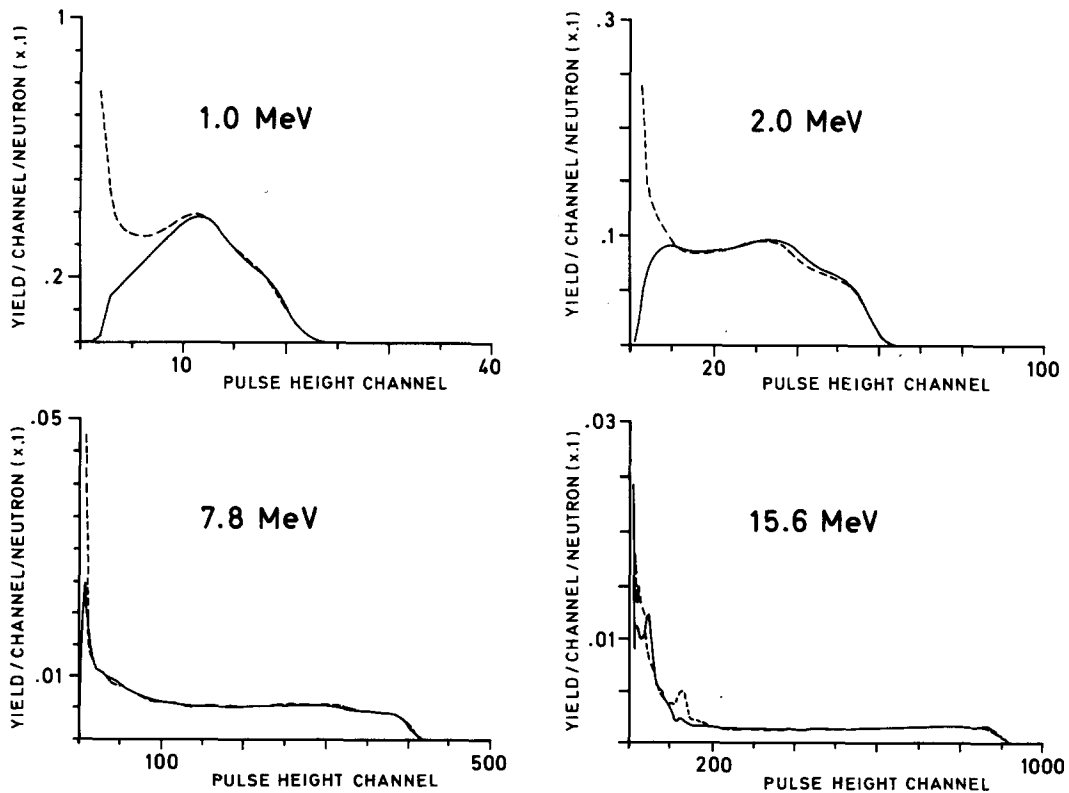


Fig. 3. Response functions for a NE213-scintillator (5 cm \times 5 cm). The experimental spectra (full line) measured at GELINA are compared with response functions calculated with the Monte Carlo code NRESP4 (dotted line). The measured curves have been normalised to the calculated spectra in the proton-recoil plateau region. The discrepancies below 700 keV proton energy are due to an imperfect pulse shape discrimination. The structure in the 15.6 MeV response function below pulse-height channel 200 is due to α -producing reactions with carbon in the scintillator.

due to the fact that both the total production cross section as well as the energy and angular distributions of the α -particles are not well known at incident neutron energies above 10 MeV [12].

3.3. Efficiencies

Absolute efficiencies were determined using pulsed monoenergetic neutron beams produced with the 7 MV Van de Graaff accelerator at the C.B.N.M. First, a relative efficiency curve was established in the energy range 0.6–7.5 and 13–16 MeV by relying on the differential neutron production cross sections [14] for the $T(p,n)^3\text{He}$, $D(d,n)^3\text{He}$ and $T(d,n)^4\text{He}$ reactions. The integrated charge on the neutron producing targets was used as monitor for the beam intensity. These relative efficiencies were converted to absolute efficiencies by measuring the incident neutron flux at five of these energies with a calibrated proton-recoil telescope [15].

Table 2 lists measured and calculated efficiencies for two different bias values. At lower energies we find increasing discrepancies with the calculations due to an imperfect pulse shape discrimination. At higher energies the agreement is very good, especially for a high bias value of 5.6 MeV proton energy where we only take into account integrals over the proton-recoil plateau.

3.4. Response matrix

For the construction of the response matrix we have used the pulse-height distributions measured at

Table 2
Comparison between measured and calculated efficiencies (%) for a NE213-scintillator ($\varnothing = 5$ cm, $h = 5$ cm)

| Neutron energy (MeV) | Low bias (300 keV) | | High bias (5.6 MeV) | |
|----------------------|--------------------|------------|---------------------|------------|
| | Measured | Calculated | Measured | Calculated |
| 0.6 | 33.9±2.8 | 48.5 | | |
| 0.8 | 40.2±3.2 | 51.9 | | |
| 1.0 | 43.0±2.4 | 50.9 | | |
| 1.2 | 43.8±2.3 | 50.3 | | |
| 1.4 | 44.7±2.6 | 49.0 | | |
| 1.6 | 43.5±2.5 | 47.9 | | |
| 1.8 | 43.0±2.2 | 46.2 | | |
| 2.0 | 42.4±2.5 | 44.6 | | |
| 2.5 | 41.1±2.4 | 42.4 | | |
| 3.0 | 39.0±1.5 | 39.5 | | |
| 4.5 | 33.7±1.2 | 32.8 | | |
| 6.0 | 30.3±1.1 | 28.3 | 2.2±0.08 | 1.9 |
| 7.5 | 26.1±1.6 | 25.2 | 7.3±0.5 | 6.8 |
| 13.0 | 22.5±1.5 | 21.8 | 9.5±0.6 | 9.3 |
| 13.5 | 21.8±1.4 | 21.4 | 9.3±0.6 | 9.2 |
| 14.0 | 21.1±1.2 | 21.6 | 9.2±0.5 | 9.1 |
| 14.5 | 20.9±0.8 | 21.8 | 9.0±0.4 | 8.9 |
| 15.0 | 20.0±1.2 | 21.7 | 8.7±0.5 | 8.8 |
| 16.0 | 19.5±1.2 | 21.8 | 8.2±0.5 | 8.5 |

GELINA. The efficiencies have been determined by taking the calculated efficiencies for a bias setting just below the proton-recoil plateau and extrapolating these down to the experimental bias relying on the shape of the measured spectra. These response functions are compressed into spectra of 1K channels of constant pulse-height width. In this way we keep at least 3 channels per fwhm of the scintillator's pulse-height resolution for proton energies above 1 MeV. The problem of an imperfect pulse shape discrimination at lower pulse-heights is bypassed by applying the same PSD setting during the scattering experiment as we used for the measurement of the response functions. The loss of neutrons will then be compensated through the unfolding.

4. Data reduction

After subtracting the sample-independent background measured with a dummy vacuum tube, the pulse-height distributions are unfolded. We use the FORIST-code [16] together with the response matrix whose construction is described in the previous paragraph. The secondary energy spectra then are corrected for self-screening and for multiple scattering in the sample and for attenuation of the emitted neutrons by the sample and by the 1.5 mm thick wall of the aluminium vacuum tube. The Monte carlo code that we have written for the calculation of the multiple scattering corrections only takes into account the elastic scattering component which in many cases is the most important contribution to the total amount of emitted neutrons. Moreover, the third interaction is considered as an absorption. These approximations are permitted because very thin samples (transmission > 0.9) are used. From these secondary energy spectra we subtract a small sample-dependent background, which we assume to be constant as function of secondary energy. The magnitude of this correction is discussed in section 5.2.

The double-differential neutron-emission cross section is calculated by the relation

$$\begin{aligned} \frac{d^2\sigma}{dE_n d\Omega}([E_k, E_{k+1}]; E_{n'}, \Omega) &= \frac{Y([E_k, E_{k+1}]; E_{n'}, \Omega) C(k) DT(k)}{\Phi([E_k, E_{k+1}]) n \Omega} \\ &= \frac{Y([E_k, E_{k+1}]; E_{n'}, \Omega) C(k) DT(k)}{n} \\ &\quad \times \frac{\sigma_r([E_k, E_{k+1}]) \epsilon g}{F([E_k, E_{k+1}]) \Omega}, \end{aligned} \quad (3)$$

where

$[E_k, E_{k+1}]$ = energy interval for incident neutrons from TOF group k ($k = 1, \dots, 32$);

- $Y([E_k, E_{k+1}]; E_n, \Omega)$ = number of secondary neutrons emitted per unit energy with energy E_n , in a solid angle Ω , corrected for background, finite sample effects and attenuation;
- Ω = solid angle of the NE213-scintillator;
- $DT(k)$ = dead time correction for TOF group k ;
- $C(k)$ = correction for losses due to coincidences;
- $\Phi([E_k, E_{k+1}])$ = integrated incident neutron flux on the sample in the energy interval $[E_k, E_{k+1}]$;
- $F([E_k, E_{k+1}])$ = number of counts in the fission chamber in the energy interval $[E_k, E_{k+1}]$;
- $\sigma_f([E_k, E_{k+1}])$ = ^{235}U fission cross section in the energy interval $[E_k, E_{k+1}]$;
- ϵ = fission product detection efficiency;
- g = constant containing the number of ^{235}U nuclei in the fission chamber layers and a geometry factor to obtain the flux at the sample position;
- n = number of nuclei in the scattering sample.

The normalisation factor $\epsilon g/\Omega$ is determined by measuring the ^{12}C differential elastic yield below 2 MeV. In this energy region the ^{12}C differential elastic cross section is known with uncertainties in the order of $\pm 1 \sim 2\%$ [17]. The flux shape measurement with the ^{235}U -fission chamber (section 2.1.) is used to extrapolate the normalisation above 2 MeV where larger uncertainties exist in the carbon differential data. With this normalisation procedure, uncertainties in the absolute efficiencies of our scintillators cancel out and only uncertainties in the relative efficiencies affect the measurement of secondary neutrons. The carbon sample thickness is chosen such as to have about the same transmission as the material sample studied. In this case the corrections for finite sample effects, background, dead time and losses due to coincidences have nearly the same magnitudes for both measurements. Possible systematic errors in these corrections will cancel out partly through the normalisation procedure.

5. Performance

5.1. General

Instabilities in the PSD which are adjusted every 24 h, still influence the pulse-height distributions below 700 keV proton energy. As a consequence, below this

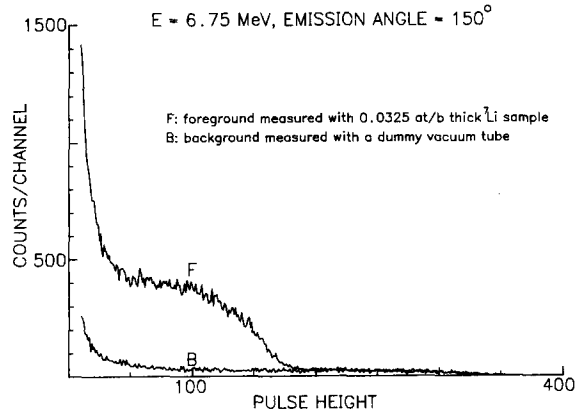


Fig. 4. Example of measured pulse-height distributions for one angle and for a specific incident neutron energy E showing the relative importance of the sample-independent background. The normalisation of the background to the foreground spectrum is explained in the text (section 2.1).

threshold the secondary neutron energy spectra become unreliable. Gain drifts for the eight detectors are checked every week. Their effect on the pulse-height resolution can be neglected.

The incident energy resolution is fixed by the width of the incident energy bins. The extent of these energy intervals is governed by the need to get adequate counting statistics in the pulse-height spectra. Below 10 MeV incident neutron energy, 0.2 to 0.5 MeV intervals are typical. Above 10 MeV, at least 1 MeV intervals are required.

The secondary energy resolution is determined by the scintillator's pulseheight resolution and by a broadening due to the unfolding procedure itself. The fwhm

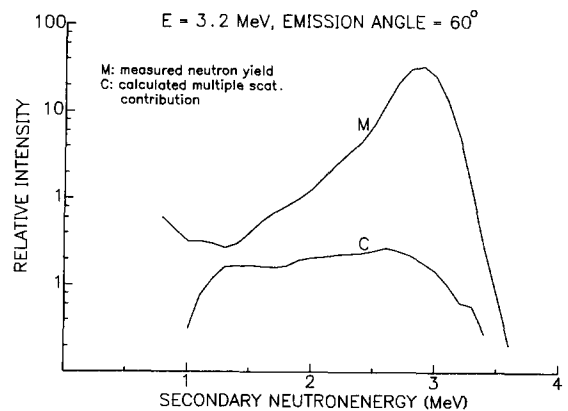


Fig. 5. Example of a measured secondary neutron energy spectrum M for one angle and for a specific incident neutron energy E together with the calculated multiple scattering contribution C. The sample was a metallic ^7Li plate ($\varnothing = 7$ cm, thickness = 0.0325 at/b).

of the Gaussian smoothing functions used in the FORIST-code varies from 40% at 600 keV to 10% at 16 MeV and is the largest factor contributing to the energy resolution. Moreover, FORIST uses an iterative smoothing technique which means that the widths of these Gaussian smoothing functions are subject to small variations dependent both on the shape of the energy spectrum and on the statistical accuracy of the pulse-height spectra. Typical energy differences, ΔE (calculated as four standard deviations), required for two scattered neutron groups to be completely resolved are $\Delta E = 1.2$ MeV at 1 MeV and $\Delta E = 3.2$ MeV at 16 MeV (here we also took into account an additional spread due to an incident energy window of 0.5 MeV). For

experiments performed with monoenergetic neutron beams where the secondary energy is determined by the time-of-flight method, these ΔE values are typically in the order of resp. 0.2 and 1.5 MeV [18].

5.2. Example: the ${}^7\text{Li}(n, xn)$ reaction

The sample was a metallic ${}^7\text{Li}$ plate, enriched to 99.97% with a thickness of 0.0325 at/b. An 8 mm depleted uranium filter was used to reduce the gamma-flash which was detected in about 45% of the linac bursts. For this first experiment only 6 detectors were available. They were located at 20 cm from the lithium sample at emission angles of 24° , 40° , 60° ,

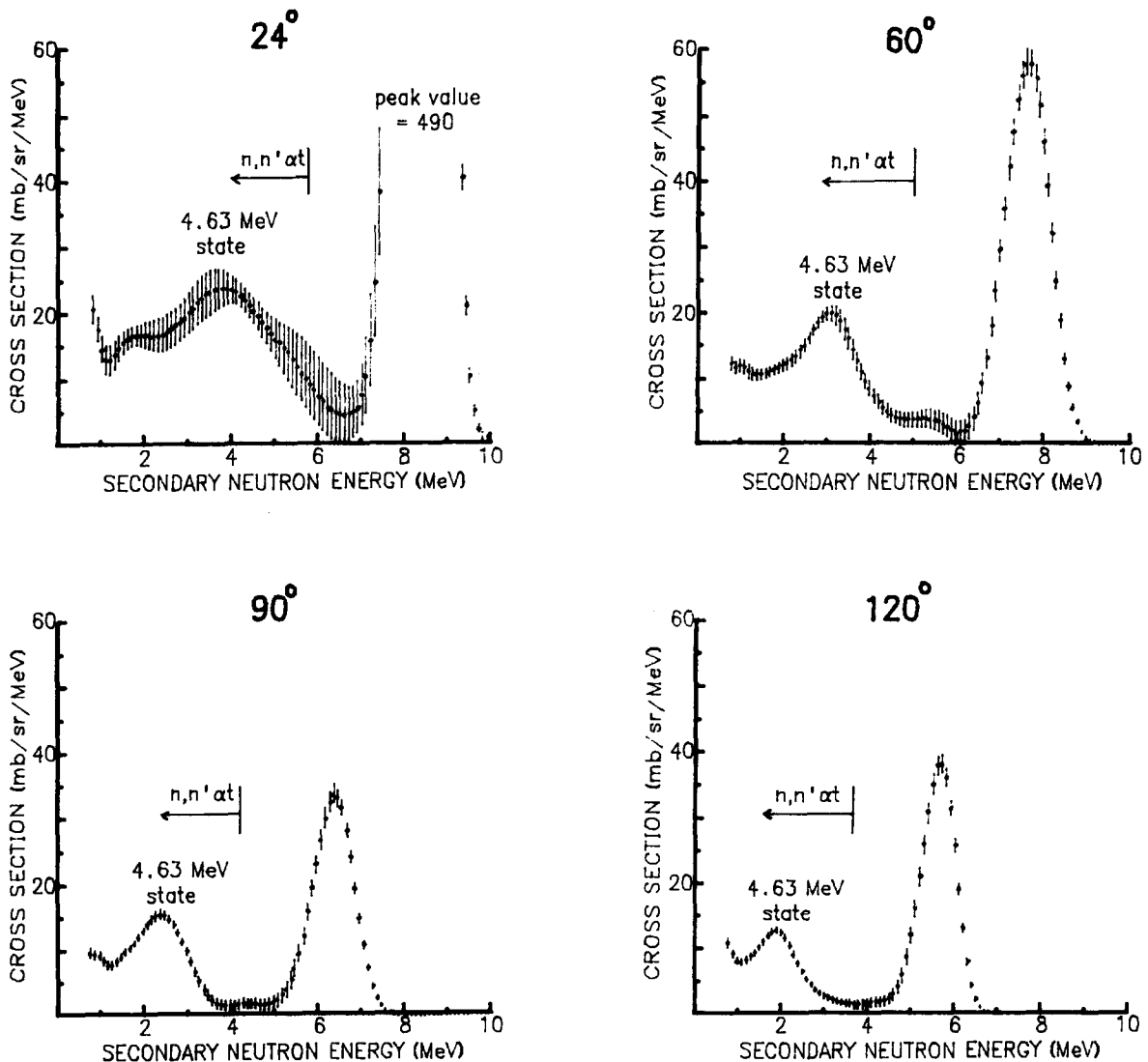


Fig. 6. Example of measured double-differential neutron-emission cross sections for incoming neutron energies between 8.4 and 8.7 MeV and for 4 angles. The error bars on the data points are statistical uncertainties calculated by the FORIST-code.

Table 3
 ${}^7\text{Li}(n, xn)$ reactions

| Reaction | Q-value (MeV) |
|---|---------------|
| 1. ${}^7\text{Li}(n, n){}^7\text{Li}$ | 0.0 |
| 2. ${}^7\text{Li}(n, n'){}^7\text{Li}^* \rightarrow {}^7\text{Li} + \gamma$ | -0.478 |
| 3. ${}^7\text{Li}(n, n'\alpha)t$ | -2.46 |
| 4. ${}^7\text{Li}(n, t){}^5\text{He} \rightarrow \alpha + n'$ | -3.42 |
| 5. ${}^7\text{Li}(n, n'){}^7\text{Li}^* \rightarrow \alpha + t$ | -4.63 |
| | -6.54, ... |
| 6. ${}^7\text{Li}(n, 2n){}^6\text{Li}$ | -7.25 |
| 7. ${}^7\text{Li}(n, 2nd)\alpha$ | -7.82 |

90°, 120° and 150°. The total average count-rate was about 0.5 events per burst (gamma-flash pulses included). The ratio of the sample-independent background to the foreground for the backward angle at 150° (worst case) varied from 20% at 10 MeV incident neutron energy to 4% at 2 MeV (fig. 4). For the forward angle at 24° this was respectively 3.5 and 2.7%. Fig. 5

shows the contribution of the multiple scattering correction which is very small.

Data were taken during 600 h [19,20] corresponding with two consecutive periods of 1 month. Above 10 MeV, even with 1 MeV incident energy-windows, the present data did not yet have the required statistical precision for unfolding the pulse-height spectra. As was mentioned in section 2.1, a new neutron producing target which will produce a harder neutron spectrum is under construction. As an illustration, we show on fig. 6 our results for the double-differential neutron-emission cross sections for an incident energy-window between 8.4 and 8.7 MeV and for four angles. The contributions from elastic and inelastic scattering to the 478 keV state (table 3) are not separated. Superimposed on the continuum part from the ${}^7\text{Li}(n, n'\alpha)t$ reaction one can identify the inelastic peak from the 4.63 MeV state. We have marked the maximum allowed energy for the continuum neutrons. The valley between the elastic peak and this continuum part illustrates how small the contribution of the sample-dependent background is. Assuming a flat energy dependence for this background it appears to be on the average 6% of the total secondary neutron yield.

6. Uncertainty analysis

The sources of uncertainty in the double-differential neutron-emission cross sections can be split in three main parts (typical values for their magnitudes are given in %):

- (a) uncertainties in the corrected secondary neutron yield due to (apart from statistical uncertainties)
- relative efficiency $\pm 2\%$ above 1 MeV
 - background subtraction $\pm 1\%$ for elastic scattering part
 $\pm 5\%$ for nonelastic scattering part (fully correlated between the different data points)
 - sample-detector distance $\pm 1\%$
 - correction for attenuation in the sample and the Al vacuum tube (5% of the correction) $\pm 1 \sim 2\%$
 - multiple scattering correction (half of the correction) $< \pm 3\%$
 - losses due to coincidences $\pm 1\%$
 - sample thickness $\pm 0.01\%$
- (b) uncertainties in the shape of the incident neutron flux due to (apart from statistical uncertainties)
- ${}^{235}\text{U}$ -fission cross section (ENDF/B-v) $\pm 2.5\%$ at 1 MeV to $\pm 6\%$ at 16 MeV
- (c) an overall normalisation uncertainty due to
- corrected differential elastic yield for the ${}^{12}\text{C}$ measurement (see (a))
 - standard differential elastic scattering cross section for ${}^{12}\text{C}$ below 2 MeV $\pm 1 \sim 2\%$
 - monitor (measured yield in the fission chamber) $\pm 3\%$

7. Conclusions

The method described here was developed to measure double-differential neutron-emission cross sections for a broad incident neutron energy range and for several angles simultaneously. For this reason an elec-

tron linac with uranium target was used as pulsed white neutron source. The energy determination of the secondary neutrons by pulse-height analysis has been very successful. The response matrix was constructed from experimentally determined response functions. The secondary energy resolution is not as good as obtained in

experiments using monoenergetic neutron beams where the secondary energy is determined by time-of-flight. In fact this secondary energy resolution depends to a large extent, through the unfolding process, on the available statistical accuracy of the pulse-height spectra.

The measurements with ^7Li have proven that, with the presently available neutron-producing target, the required statistical accuracy can be obtained in a reasonable measuring time, at least up to 10 MeV incident neutron energy. This measuring time is less crucial with a white neutron source because the installation can be used for several experiments at the same time. To be competitive with monochromatic neutron sources above 10 MeV, a new neutron producing target consisting of a U-Be mixture, which will produce a harder neutron spectrum than the currently used uranium target, is under construction.

The same experiments with ^7Li have also demonstrated the very favourable background conditions (because of the large source-detector distance of 60 m). For this reason very thin samples ($T > 0.9$) may be used so that the multiple scattering effect in the sample involves only small corrections. The overall uncertainty in the measured cross sections will be less than $\pm 10\%$ which is within the requirements for fusion applications.

For the future measurements we plan to extend the data acquisition software to store simultaneously the information for neutron and gamma events in two separate three-dimensional arrays (detector \times time-of-flight \times pulse-height). In this way we will obtain additional information on inelastic channels where gamma rays are emitted by the excited nuclei. It will allow separation of elastic scattering from inelastic scattering to low-lying levels even though the secondary neutron energy resolution is too poor to resolve the different contributions.

Acknowledgements

The authors wish to thank the operating teams of the Van de Graaff and linear electron accelerators of the C.B.N.M., the staff from the workshop and the electronic groups of the S.C.K./C.E.N. and C.B.N.M., in particular P. D'Hooghe and S. De Jonge. We wish to thank J. Van Audenhove and E. Freistedt for the preparation of the samples. The help of J. Pagggers and R. Widera during the experimental work is greatly appreciated.

References

- [1] World Request List for Nuclear Data, Report INDC (SEC)-78/URSF (1981).
- [2] R.C. Haight, in: Proc. Int. Conf. on Nuclear Cross Sections for Technology, Knoxville, NBS Special publication n° 594 (October 1979) 228.
- [3] O.N. Jarvis, European Applied Research Reports-Nucl. Sci. Technol., (1, 2) (1981) 127.
- [4] M.A. Abdou, in: Proc. Int. Conf. on Nuclear Data for Science and Technology, Antwerp (September 1982) 293.
- [5] G.L. Morgan, T.A. Love and F.G. Perey, Nucl. Instr. and Meth. 128 (1975) 125.
- [6] D. Tronc, J.M. Salomé and K.H. Böckhoff, Nucl. Instr. and meth. 228 (1985) 217.
- [7] J.M. Salomé and R. Cools, Nucl. Instr. and Meth. 179 (1981) 13.
- [8] F. Corvi, L. Calabretta, M. Merla, T. van der Veen and M.S. Moore, Proc. of the NEANDC/NEACRP Spec. Meeting on Fast-Neutron Capt. Cross Sect. (April 1982) 347.
- [9] G. Dietze and H. Klein, PTB-Bericht, NRESP4 and NEFF4 - Monte Carlo Codes for the Calculation of Neutron Response Functions and Detection Efficiencies for NE213-Scintillation Detectors, PTB-ND-22 (October 1982).
- [10] C.R. Jungmann, H. Weigmann, L. Mewissen, F. Poortmans, E. Cornelis and J.P. Theobald, Nucl. Phys. A386 (1982) 287.
- [11] G. Dietze and H. Klein, Nucl. Instr. and Meth. 193 (1982) 549.
- [12] G. Dietze, H.J. Brede, H. Klein and H. Schölermann, Proc. of Fourth Symp. on Neutron Dosimetry, EUR 7448 (1981) 373.
- [13] H. Schölermann and H. Klein, Nucl. Instr. and Meth. 169 (1980) 25.
- [14] H. Liskien and A. Paulsen, Nucl. Data Tables 11 (1973) 569.
- [15] H. Liskien, Proc. Symp. on Neutron Standards Flux Normalisation, Argonne, AEC-Symposium Series 23 (1970) 343.
- [16] R.H. Johnson, FORIST, Neutron Spectrum Unfolding Code, Radiat. Shield. Inf. Center, Computer Code Collection PSR-92, ORNL (1975).
- [17] C.Y. Fu and F.G. Perey, At. Data and Nucl. Data Tables 22 (1978) 249.
- [18] H.H. Hogue, PhD Thesis, Duke University (1977) unpublished.
- [19] E. Dekempeneer, H. Liskien, L. Mewissen and F. Poortmans, Proc. Int. Conf. on Nucl. Data for Basic and App. Science, Santa Fe, New Mexico (May 1985).
- [20] E. Dekempeneer, H. Liskien, L. Mewissen and F. Poortmans, Proc. Int. Conf. Fast Neutron Physics, Dubrovnik, Yugoslavia (May 1986).